Gold promoted Cu/ZnO/Al$_2$O$_3$ catalysts prepared from hydrotalcite precursors: Advanced materials for the WGS reaction

J.L. Santos [a], T.R. Reina [a,b,*], S. Ivanova [a], M.A. Centeno [a], J.A. Odriozola [a]

[a] Departamento de Química Inorgánica, Universidad de Sevilla e Instituto de Ciencias de Materiales de Sevilla Centro Mixto US-CSIC Avda, Américo Vespucio 49, 41092 Seville, Spain
[b] Department of Chemical Engineering and Process Engineering, University of Surrey, Guildford, GU2 7XH, United Kingdom

ABSTRACT

Outstanding catalysts for the water was shift reaction are reported in this work. The combination of gold nanoparticles with Cu/ZnO/Al$_2$O$_3$ prepared from hydrotalcite-like precursors leads to very promising systems for pure hydrogen production. Full CO conversion is reached at temperatures as low as 180 °C. The key point seems to be the cooperation of Au and Cu and the optimal metal-oxide contact derived from the synthesis method. The high activity of gold for low temperature CO oxidation and the suitability of copper for the WGS results in a perfect synergy. Moreover the materials developed in this work present good stability and tolerance towards start/stop cycles an indispensable requisite for a realistic application in an integrated hydrogen fuel processor.

© 2016 Elsevier B.V. All rights reserved.

1. Introduction

Despite its more than 200 years of history the water gas shift (WGS) reaction still represents a challenge for chemists working in catalysis. The renewed interest in the process is been guided by the ongoing world-wide politics aiming to ensure a greener energy future [1]. In particular, the WGS reaction is intimately linked to the development of H$_2$ alimented fuel cells. Proton exchange membrane (PEM) fuel cells are devices able to convert the chemical energy of H$_2$ into electricity generating exclusively water as by-product [2–4]. The use of fuel cells for portable applications involves a series of stages including the production of hydrogen via reforming of hydrocarbons [5–7] or biomass feedstock [7] and subsequent hydrogen purification via WGS, preferential CO oxidation and/or methanation to remove the CO produced in the reforming process [8].

Among the CO elimination steps, the WGS (CO + H$_2$O ↔ CO$_2$ + H$_2$) is the most relevant in terms of CO concentration in the inlet of the reactor. Furthermore, successful WGS process leads not only to CO depletion but also increases the hydrogen concentration in the gaseous stream. Hence, the development of highly efficient WGS catalysts is essential to guarantee the success of hydrogen economy.

Part of the mystery of this reaction resides on its thermodynamic and kinetics features. The shift process is an exothermic equilibrium limited reaction which implies that the CO conversion drops upon increasing the temperature. Therefore in principle, it is more desirable to work at low temperatures. However, the reaction rates are rather low in this temperature regime avoiding high conversions. In order to overcome this conflict, industrially the reaction is carried out in two separate adiabatic reactors involving a high temperature WGS step followed by a second low temperature WGS process [9]. The most successful catalytic formulation for the low temperature WGS are based on Cu/ZnO/Al$_2$O$_3$ mixtures. The active phase of this system is Cu while ZnO and Al$_2$O$_3$ are mend to stabilize and avoid copper particles sintering and sulfur poisoning [9,10]. In particular, ZnO is a very efficient additive to prevent copper sulphidation since in the low temperature water gas shift range the sulphidation of ZnO (ZnO + H$_2$S ↔ ZnS + H$_2$O ΔH = −76.7 kJ/mol) is rather favored [9]. An extra advantage of the ZnO is its possibility to form oxygen vacancies during the WGS reaction [11]. These oxygen defects may also influence the catalytic activity since they facilitate water activation, which is the rate limiting step [11]. Despite its commercial application, the preparation of Cu/ZnO/Al$_2$O$_3$ catalyst is not yet fully understood [12]. Recently, the use of Cu, Zn, Al hydrotalcite-like compounds has been proposed as an ideal precursor of the Cu/ZnO/Al$_2$O$_3$ catalyst leading a con-

trol microstructure with enhanced metal-oxide interactions and high metallic dispersion [12]. Although the Cu based catalysts prepared from hydrotalcite-like precursors presents attractive skills for the WGS, the nature of the $Cu/ZnO/Al_2O_3$ system imposes several drawbacks including pyrophoricity and obligatory activation steps [13,14].

In order to avoid these problems noble metal based catalysts are under intensive investigation [15–17]. Within the noble metals, gold is a rather promising alternative. Very active WGS catalysts are obtained when gold is supported on reducible materials specially ceria and promoted ceria [18,19]. To the best of our knowledge, the combination of gold with the $Cu/ZnO/Al_2O_3$ formulation has not been considered. In this sense, the aim of this paper is to develop very efficient WGS catalysts for pure hydrogen production by combining two active systems: small and well dispersed gold nanoparticles plus $Cu/ZnO/Al_2O_3$ mixtures prepared from hydrotalcite precursors.

2. Experimental

2.1. Catalysts preparation

2.1.1. $Cu/ZnO/Al_2O_3$ mixtures

Catalysts based on $Cu/ZnO/Al_2O_3$ mixtures were obtained by the co-precipitation process at low saturation as described elsewhere [20]. Aqueous solutions of the metallic precursors $Cu(NO_3)_2 \cdot 2H_2O$, $Zn(NO_3)_2 \cdot 6H_2O$, $Al(NO_3)_3 \cdot 9H_2O$ (Sigma Aldrich) with the necessary amount to obtain the intended Cu/Zn ratio were prepared. Later, an aqueous solution of (Sigma Aldrich) 1M Na_2CO_3, was added dropwise to the Cu/Zn/Al mixture in order to obtain the pH of 8 [21]. Constant pH was maintained during 48 h using an automatic burette (Crisol pH-Burette 24). After the precipitation the solution was filtered and dried in oven at 90 °C overnight. Under this procedure three hydrotalcite supports were prepared with Cu/Zn ratio of 1.4, 2.8 and 5.6.

Finally the hydrotalcites were calcined in air at 300 °C for 4 h at 10 °C/min leading to the mixed oxides structures. For sake of simplicity the obtained mixed oxides from the hydrotalcites precursors are labelled HT 1.4; HT 2.8; HT 5.6, with the Cu/Zn ratios indicated.

2.1.2. Gold deposition

For the gold addition, the mixed oxides were sieved and the 100–200 μm fractions retained were used to prepare the gold based catalysts. The gold deposition was performed by the direct anionic exchange method (DAE) [22] assisted by NH_3. Aqueous solutions of the gold precursor $HAuCl_4$ (Johnson Matthey) 2×10^{-4} M were used in order to obtain a final Au loading of 1 wt.%. The solution was heated to 70 °C and aged 20 min. After that the solution was cooled down to 40 °C and 50 mL of NH_3 (30% Aldrich) were added. The slurry was then filtered, washed with water, dried in an oven at 100 °C overnight. Finally the solids are calcined in air at 350 °C for 4 h. The gold promoted catalysts are labelled as Au/HT 1.4; Au/HT 2.8 and Au/HT 5.6 in agreement with the nomenclature employed for the mixed oxides solids.

2.2. Characterization techniques

The chemical composition of the samples was determined by X-Ray micro fluorescence spectrometry (XRMF) in an EDAX Eagle III spectrophotometer with rhodium source of radiation.

The Temperature Programmed Reduction (TPR) experiments were carried out in conventional quartz reactor connected to a thermal conductivity detector (TCD) calibrated with a CuO standard (99.999%). The reactive gas stream, 5% H_2 in Ar (Air Liquide) was passed through a 50 mg of sample with a flow rate of 50 mL min^{-1} and the temperature rose at 10 °C min^{-1} from room temperature to

Table 1
Experimental conditions of the catalytic tests.

	Model	Realistic
CO (vol.%)	4.5	9
H_2O (kPa)	31.1	31.1
CO_2 (vol.%)	–	11
H_2 (vol.%)	–	50
N_2 (vol.%)	Balance	–
Bed volume (cm^3)	1.5	1.5
GHSV (h^{-1})	4000	4000

Table 2
Chemical composition of the prepared mixed samples.

Sample	Au% (w/w)	CuO% (w/w)	ZnO% (w/w)	Al_2O_3 % (w/w)	CuO/ZnO
HT 1.4	–	35.82	25.97	38.21	1.38
HT 2.8	–	47.73	17.40	34.87	2.74
HT 5.6	–	51.95	10.34	37.71	5.02
AuHT 1.4	1.05	35.74	25.81	37.40	1.38
AuHT 2.8	0.93	41.03	15.18	42.80	2.70
AuHT 5.6	1.2	43.57	8.70	46.60	5.01

900 °C. Molecular sieve 13× was used to retain the H_2O produced during the reduction.

Raman spectroscopy measurements were performed on Horiba Jobin Yvon dispersive microscopy (HR800) with confocal aperture 1000 μm, using a laser spot diameter of 0.72 μm and spatial resolution of 360 nm. The microscope is equipped with a diffraction grating of 600 grooves/mm, and a CCD detector, using a green laser (λ = 532.14 nm, maximum power 20 mW) and a 100× objective.

FTIR spectra were recorded in a Jasco FTIR 6200 IRT-5000 equipment. Spectra were collected at 4 cm^{-1} resolution in transmission mode (samples diluted 1/100 in KBr).

X-ray diffraction (XRD) analysis was carried out on an X'Pert Pro PANalytical instruments. Diffraction patterns were recorded using Cu Kα radiation (40 mA, 45 kV) over a 2θ-range of 10–90° and a position-sensitive detector using a step size of 0.05° and a step time of 240 s.

2.3. Catalytic activity

Water gas shift reaction was performed in a 304 stainless steel flow reactor (internal diameter of 0.75 cm) at atmospheric pressure in the 160–350 °C temperature range, using two reaction mixtures named model and realistic conditions (Table 1). The model reaction mixture is the one usually employed for clean H_2 production via WGS. The realistic conditions simulate the outlet of an ethanol reformer and they can be designed as CO clean-up conditions. No activation procedures were employed prior the reaction. The catalysts were pelletized, sieved and the 600–800 μm fraction is used the tests. The CO and CO_2 content was analysed with an on-line ABB gas analyser and the activity expressed in terms of CO conversion.

3. Results and discussion

3.1. Chemical composition

The measured chemical composition of the prepared samples expressed in% (w/w) is presented Table 2. As shown in the table the actual compositions of the mixed oxide match well the targeted ones, indicating the suitability of the implemented preparation method to obtain mixed oxides. The samples present a gradual increase of copper loading maintaining the desired Cu/Zn ratio for all the mixed oxides except for the HT 5.6 which copper loading is a slightly lower than the nominal value.

The addition of gold does not alter significantly the mixed oxide composition just a minor decrease of Zn and Cu was detected. The

latter is due to the highly basic media employed during the gold deposition as reported elsewhere [23]. As for the gold loading, all the gold promoted catalysts presented rather similar gold loading close the targeted 1% (w/w).

3.2. XRD

X-Ray diffraction patterns of the prepared materials at different stages of catalystís use (calcined, gold deposited, WGS reacted) are presented in Fig. 1. For instance, the XRD profiles of the fresh samples supports (Fig. 1A) revealed the presence of an hydrotalcite-like structure $(Cu,Zn)_{1-x}Al_x(OH)_2$-$(CO_3)_{x/2}$ m H_2O with typical diffractions of laminar materials such as hydrotalcites and malachite (ICDD 37-0629 and ICDD 41-1390). Similar patterns were obtained elsewhere [24,25] for hydrotalcite type structures. The d spacing at 12 and 24° 2θ corresponding to the planes (003) and (006), respectively, accounts for the full and half stacking height of brucite-like sheets [12].

After calcination the crystalline domains of hydrotalcite-like structure are no longer observed (Fig. 1B) and the obtained diffractions are ascribed to copper species mainly CuO (ICDD 48-1548), dispersed in a Zn-Al mixed oxide matrix. Despite CuO observed as dominant species, it is worth to mention that some diffractions due to Cu_2O (ICDD 03-065-3288) and Cu (ICDD 00-004-0836) were observed for the HT 2.8 sample. It seems that the decomposition of the hydrotalcite using the Cu/Zn ratio of 2.8 permits the stabilization of metallic Cu upon calcination. Also some unidentified peaks are observed and could correspond to metallic (copper or zinc) carbonates that are stable after the calcination at 350 °C. Behrens and co-workers, reported that complete decarbonatation of this type of materials requires higher temperatures above 500 °C [12].

Upon gold deposition (Fig. 1C), the diffraction pattern of all the samples resembles that of the massive CuO. Only the diffraction at 2θ = 29.8° attributed to (110) reflexion on Cu_2O appeared for HT1.4 and HT5.6. However for the HT 2.8 sample, the additional copper species (Cu_2O) are fully oxidized, due to the second calcination step on air at 350 °C after gold impregnation. Furthermore, it was not possible to detect any crystalline phase attributed to gold (ca. 38, 45 and 65° 2θ). The latter indicates good metallic dispersion and small particle size typically beyond the resolution limit of the diffractometer (<4 nm). Overall, it seems that after two calcination steps (one for the supports and one for the gold based catalysts) the samples are composed by small gold particles dispersed on mixed Cu-Zn-Al oxide matrix with well-defined CuO domains.

Finally it is interesting to study the possible phase changes due to the WGS reaction. In Fig. 1D the diffraction patterns of the some selected samples before and after reaction are shown. The reduction of CuO (pre reaction) to metallic Cu (post reaction) phase was observed indicating the presence of metallic Cu during the WGS test as component of the catalysts' active phase.

3.3. FTIR study

Structural information of the prepared materials is obtained via FTIR spectroscopy (Fig. 2A). A sharp band at 1383 cm^{-1} is observed and ascribed to residual amounts of nitrates not removed during the calcination procedure as previously reported by other authors [26]. The presence of carbonates intended from the XRD data is confirmed by IR. Well defined bands related to the antisymmetric stretching (ν_3) at 1353 cm^{-1} and the out-of-plane bending vibration (ν_2) at 822 cm^{-1} reveals carbonate presence in the HT structure. The band at 1051 cm^{-1}, better defined for the HT 1.4 sample, accounts for the symmetric ($\nu\nu_1$) carbonate mode and is due to the lower symmetry of the interlayer carbonate ions interacting with their neighbors in the mixed oxide structure [12]. This lower carbonate symmetry in the structure compared to free ions leads to

the splitting of the ($_3$) mode, explicating the band at 1497 cm^{-1}. In addition, the band centered at 1639 cm^{-1} is associated with the deformation mode of water (ν_2), chemisorbed in outer surfaces [12].

The addition of gold and the subsequent calcination at 350 °C partially removes the nitrates and carbonates from HT1.4 and HT5.6 and completely from the HT2.8, confirmed us the FTIR spectra of the gold catalysts (Fig. 2B). The HT 2.8, appears sample to be different from the other two samples, it is able to stabilize Cu and Cu_2O species before and after gold addition and various calcination steps and in the same time is the only sample free of carbonates, prior the WGS reaction.

3.4. Raman study

As the sampleís composition and more specifically the Cu/Zn ratio influences the microstructure and catalyst behavior some, Raman experiments were carry out to extract further structural information and to establish structure/activity relationship and in our materials. Raman spectra of the uncalcined samples are presented in Fig. 3A, and are characteristic for Zn-Al and Cu-Al hydrotalcite compounds. The fresh samples present the Raman modes of carbonate groups $\nu\nu_1$, ν_3 and ν_4, (1100, 1400 and 700 cm^{-1}, respectively), bands related to hydrogen-bonded OH groups of the brucite-like layers (in the 200–300 cm^{-1} range), bands related to OH—O units produced from the water bonding to carbonate groups (around 500 cm^{-1}) and metal-oxygen symmetric stretching vibrations (below 700 cm^{-1}) [27,28]. The structure of the carbonate ν_1 stretching vibration mode give us a very interesting information about the type of hydrotalcite formed (Fig. 3B). At least two Raman components are detected, one around 1055 cm^{-1} and the other at around 1100 cm^{-1}. The first one has been reported as characteristic of Zn—Al hydrotalcites and the second one of Cu—Al ones [29]. The proportion of the component at 1100 cm^{-1} decreased at higher Cu/Zn ratio, while a shift of carbonate bands position is detected. This observation indicates that the Cu—Zn—Al interaction is favored at the higher Cu/Zn ratio studied, producing a more homogenous Cu—Zn—Al hydrotalcite, while at lower Cu/Zn ratios, inhomogeneous hydrotalcites, with a composition closer to a pure Zn—Al and Cu—Al hydrotalcite, are formed. In fact, the Raman band at 1100 cm^{-1} can be directly associated to carbonate species of the malachite compounds evidenced by XRD (Fig. 1A), suggesting the segregation of part of the copper outside the hydrotalcite structure. Also, in the 1.4 HT sample, the formation of a Zn-rich hydrotalcite is confirmed by the intense bands due to Zn—O vibrations at 222, 270 and 436 cm^{-1} [27,28]. As for the calcined hydrotalcites the Raman spectra shown in Fig. 3C, most of the bands match the CuO Raman modes. For instance, the phonon at 293 cm^{-1} may correspond to the Ag mode and the peaks at 341 and 630 cm^{-1} to the B_g modes of the cupric oxide [30]. In addition to these three bands, a broad band centred at 1150 cm^{-1}, assigned to multi-phonon (MP) transition was observed [31]. Curiously, a gradual shift towards lower wavenumbers of the bands at 293 and 341 cm^{-1} was observed upon increasing copper loading. Most likely the higher concentration of copper species in the mixed oxides enhances the Jahn-Teller effect provoking greater Cu-octahedral distortion and introducing lattice strains that derive into broadening and shifting of the vibration modes. Only a small band due to carbonate groups ca. 1058 cm^{-1} appears for all the samples although it is less notable for the HT 2.8. The position of the band indicates that they are basically $ZnCO_3$ species although the existence of a certain proportion of $CuCO_3$ cannot be discarded since it appears at around 1100 cm^{-1} [28]. Regarding the bands at 416 and 730 cm^{-1} they could indicate the presence of $ZnAl_2O_4$ spinel [32]. For instance, the band at 730 cm^{-1} is assigned to an Al—O stretching vibration of AlO_4 tetrahedra while
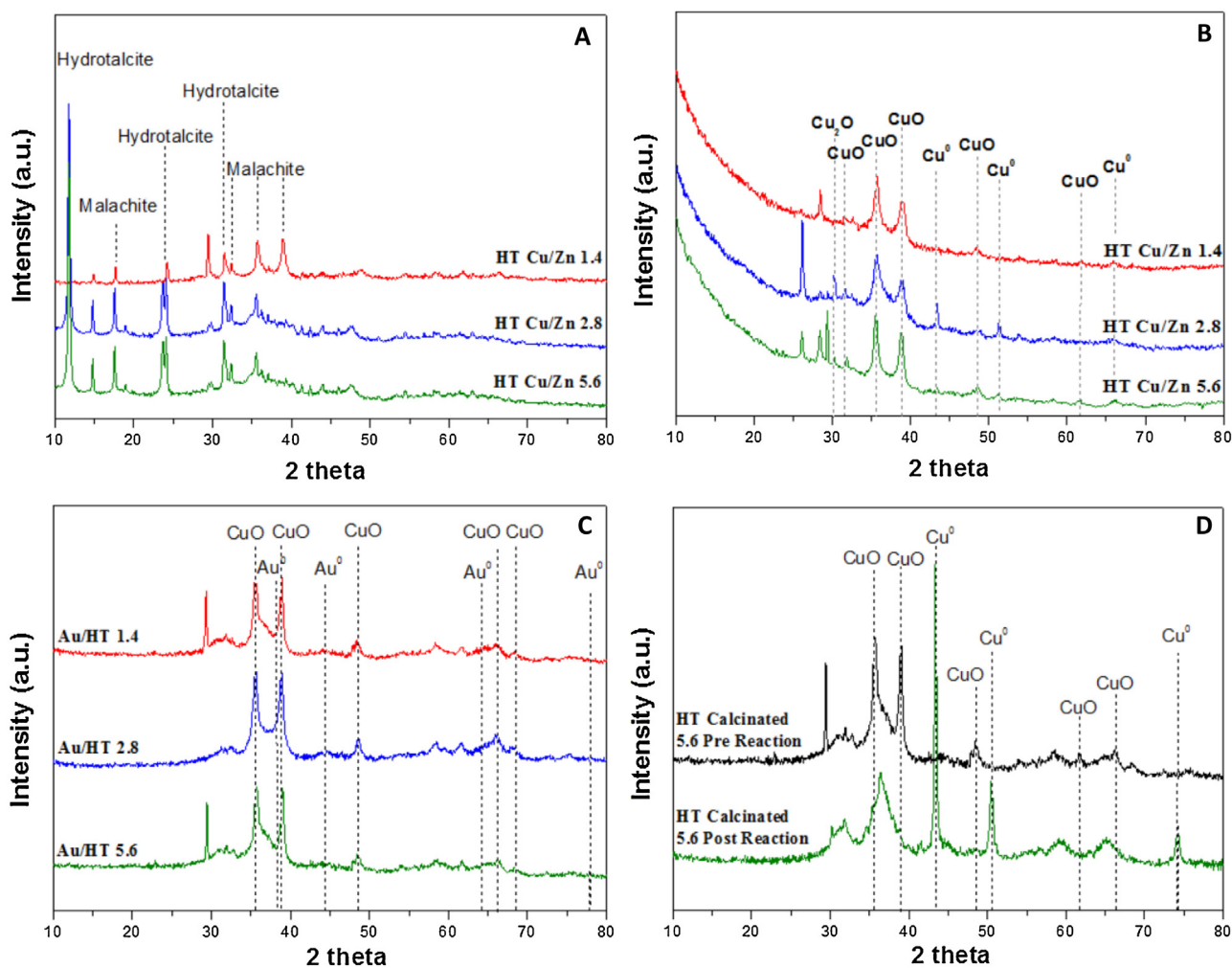
Fig. 1. XRD patterns of the studied materials. A) before calcination; B) calcined supports; C) gold based catalysts; D) pre and post reaction comparison.
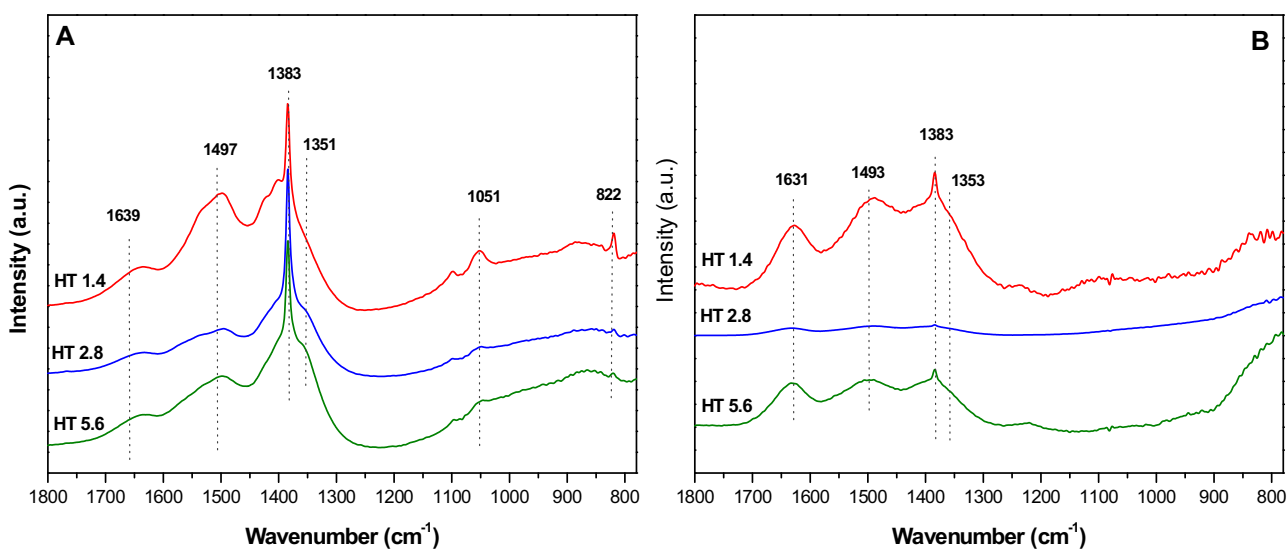

Fig. 2. FTIR spectra of the prepared samples. A) supports B) gold based catalysts.

the band at 416 cm^{-1} is assigned to the E_g mode of the spinel [33]. Spinel-type oxides are typical decomposition products of hydrotalcite precursors. Normally they crystallize at higher temperatures above 600 °C, although formation of amorphous or poorly crys-

talline nonstoichiometric spinel phases at lower temperature have been previously observed as intermediate products in course of the thermal decomposition of the layered materials [25].
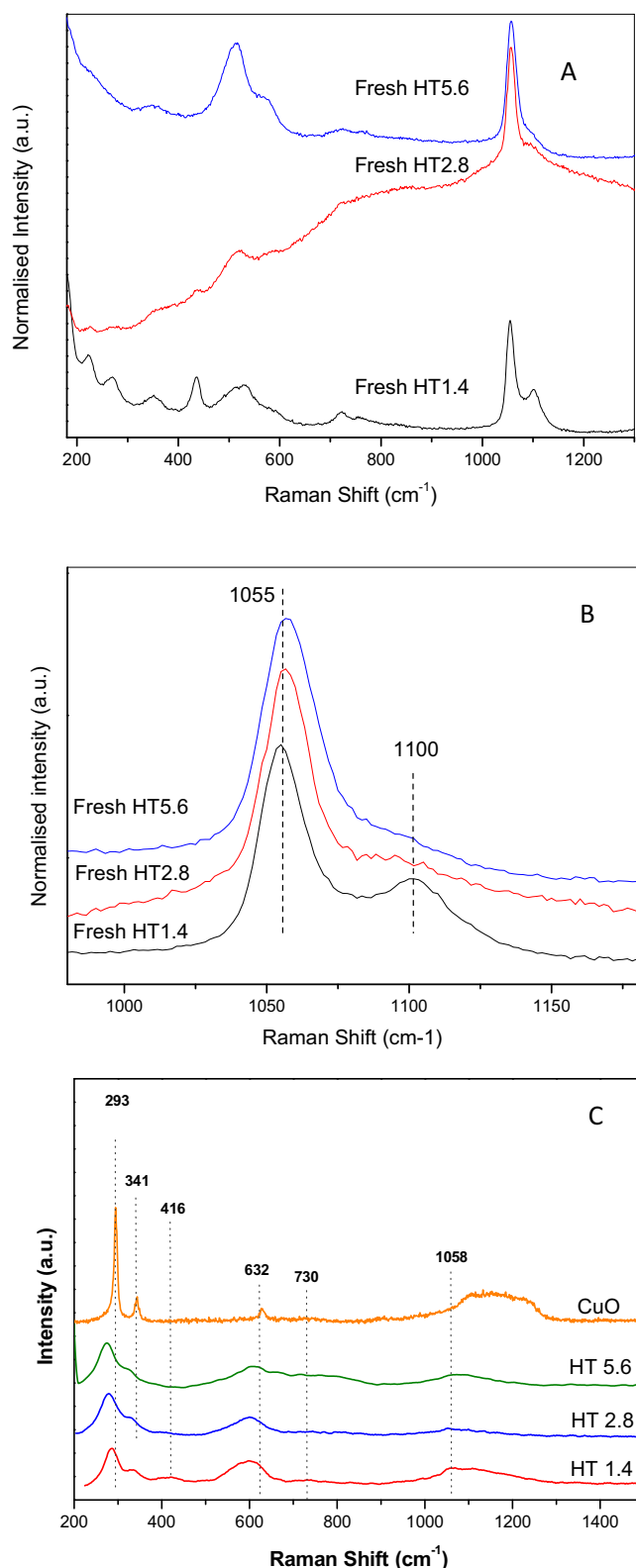
Fig. 3. Raman spectra of the mixed oxides A) and B) before calcination C) calcined supports.

In summary the characterization techniques reveal complex nature of the synthetized materials. The decomposition of the primary hydrotalcite at mild conditions (300 °C) leads to the formation of the mixed Cu—Zn—Al oxides with some carbonates and water remaining in the structure maybe due to certain degree of retention
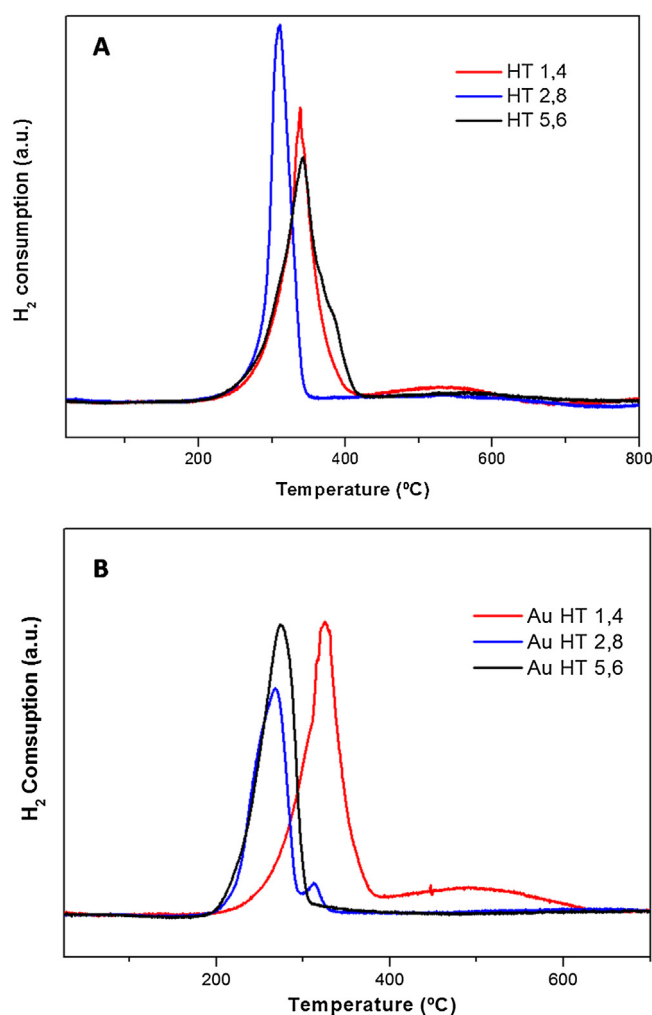

Fig. 4. H_2-TPR profiles of the prepared materials: A) supports B) gold based catalysts.

of the original laminar structure thus leaving some room for those species to be allocated on the interlaminar space. Also the laminar structure would be always a frequent configuration for this type of materials given the well-known memory effect of hydrotalcites. Gold deposition and a subsequent calcination at higher temperature (350 °C) leads to the final catalysts composed by small and highly dispersed gold nanoparticles in contact with CuO species over a matrix of ZnAl spinel.
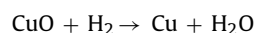
3.5. Reducibility: H_2-TPR

Redox properties are essential to understand the catalytic behavior in a redox reaction as such WGS. In this sense, to evaluate the reducibility of the catalysts H_2-TPR experiments were conducted and the results are presented in Fig. 4. Fig. 4A shows the reduction profiles of the prepared supports. The reduction zones, are associated to the reduction of Cu^{2+} (CuO) to metallic copper Cu^0. Some differences among the samples in the reducibility profile can be noticed [34,35]. For example, HT 1.4 and HT 5.6 presented a broader reduction window with a maximum centered ca. 350 °C, while the HT 2.8 reduction profile is narrower and shifted towards lower temperature indicating a higher and more homogenous reducibility for this sample. The greater redox properties of this sample agree with the XRD results in which the existence of some stabilized metallic copper was observed. In principle, the presence of the metallic Cu may facilitate the overall reduction of the mixed oxide.

In addition, as shown in the TPR profile, a second reduction process centered at about 550 °C appears for the HT 1.4. Very likely this process is due to the reduction of the segregated malachite phase observed in the sample by XRD and or carbonates reduction/decomposition.

As for the gold based catalysts the samples present a similar profile than their parent supports with some minute but interesting differences (Fig. 4B). Firstly, the main reduction zone of Au/HT 2.8 and Au/HT 5.6 are shifted to lower temperatures indicating that gold favors copper reducibility. For the Au/HT 1.4 sample the reduction events take place in almost the same temperature window observed for the support. This fact most likely indicates a weaker Au-CuO contact perhaps due to the presence of carbonates on this sample as observed by IR thus limiting the accessibility of gold to the CuO dispersed species. Also the Au/HT 2.8 sample exhibits a small shoulder at 310 °C accounting for a second reduction process probably due to bigger or less dispersed CuO particles.

For a deeper understanding of the reducibility of the samples, TPR profiles were treated quantitatively. The reducibility percentage was calculated from the integrated area of reduction peaks. Theoretical H_2 consumption is calculated considering the following process:

$$CuO + H_2 \rightarrow Cu + H_2O$$

The actual amount of CuO is derived from the XRF data and is used to calculate the experimental H_2 consumption. This experimental value is referred to a theoretical value obtained from the TPR calibration and the percentage of reducibility is obtained from the equation below. No contribution of gold oxidized species is considered in the calculation since the DAE method leads generally to metallic gold nanoparticles [22].

$$\%Reducibility = H_2experimental/H_2theoretical \times 100 \qquad (1)$$

Samples HT 2.8 and HT 5.6 are fully reduced during the experiment while HT 1.4 reached 94% of reduction. In other words, there are no big differences in terms of quantitative reducibility. Therefore the main difference that we can infer among the supports from the TPR study is the lower temperature needed to fully reduce the HT 2.8 sample pointing its better redox behavior compared to HT 1.4 and HT 5.6. On the other hand, all the gold based catalysts reached full reduction. Actually there is not a great effect of gold in the quantitative reducibility of the mixed oxides since they achieved complete reduction beforehand. Nevertheless, as commented above gold lowers the reduction temperature of the copper oxide which may cause an impact in the exhibited catalytic behavior.

3.6. Catalytic activity

The catalytic screening in the WGS reaction of the prepared hydrotalcites is presented in Fig. 5. Unlike the traditional copper zinc catalysts that require prior reduction before performing under industrial conditions, our catalysts were submitted to the catalytic tests without any previous pretreatment, a valuable issue when real applications are targeted. In addition, the catalysts were tested in two consecutive runs to ensure that the observed CO conversion was due exclusively to the WGS reaction and no parallel effects as for example CuO reduction ($CuO + CO \rightarrow CO_2 + Cu$) interferes the results.

As shown in Fig. 5, the general trend is that the conversion increases with increasing the temperature until reaching the equilibrium conversion, where the catalysts perform at the maximum conversion allowed by the thermodynamics.

It is interesting to note that the HT 1.4 sample, possess lower catalytic activity at all studied temperatures, compared to the other
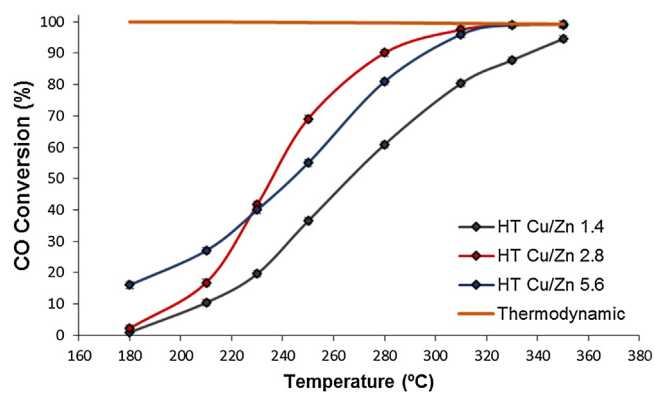

Fig. 5. Catalytic screening of the prepared supports in model WGS conditions.
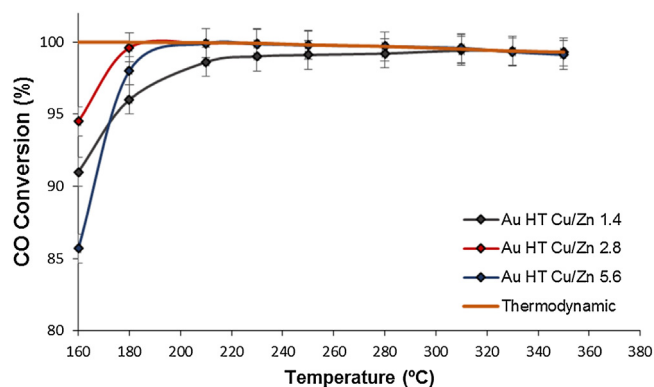

Fig. 6. WGS behavior of the prepared gold based catalysts in model WGS conditions.

two systems. Some factors may explain this poorer activity, e.g. smaller quantity of Cu on its composition (given the active role of Cu in the process) and also its poorer reducibility which in turn drives to less metallic copper available during the shift process. On the other hand, both HT 2.8 and HT 5.6 samples reached the equilibrium conversion at the same temperature (310 °C). This observation could indicate that the 2.8 presents an optimum Cu/Zn ratio that equals the performance exhibited by the HT 5.6 with half copper loading. In fact, the HT 2.8 is a special sample with the best redox features and with particular structural properties as for example the presence of Cu_2O and Cu on its composition as indicated by XRD. As metallic copper is stabilized on mixed oxide structure, this sample is ready to work in the WGS without any pretreatment. While the other two samples need to be reduced during the process, the HT 2.8 is self-activated due to its structural composition.

The effect of gold in the WGS activity of the mixed oxides is analyzed in Fig. 6. The results clearly show the strong impact of the noble metal in the process increasing dramatically the conversion especially at low temperatures.

All the samples reached more than 80% of CO conversion at low temperatures (160 °C) and equilibrium conversion at 180 °C, an unprecedented result in the literature involving gold based catalysts for WGS. Several reasons may account for the fairly good performance exhibited by these catalysts: (i) The high activity of nanogold based catalysts for the CO oxidation especially when supported on reducible oxides [36–38]; (ii) the suitability of Cu–Zn–Al mixed oxides for the WGS when prepared from hydrotalcite-like precursors driving to an optimum microstructure and metallic dispersion. These types of oxides are indeed the most extended commercial catalysts for the low temperatures water gas shift reactors [37]; (iii) the synergy established between gold nanoparticles and mixed oxides; in such a way that gold enhances Cu reducibil-

Table 3

WGS specific reaction rates at 180 °C. All the values are referred to the amount of active phase which is considered the sum in moles of Au and Cu.

Sample	WGS rates (mol CO converted/s × mol active phase × 10^{-4})
HT 1.4	0.14
HT 2.8	0.16
HT 5.6	0.15
AuHT 1.4	6.70
AuHT 2.8	6.26
AuHT 5.6	5.80
Au/CuCe bulk [42]	1.31

Fig. 7. WGS behavior of the prepared gold based catalysts in post-reforming mixtures.

Fig. 8. Long thermal stability test of the most active sample.

ity, leading to the formation of the active phase (metallic copper) at early reaction stages and high performances at low temperatures (iv) the co-existence of two active phases, gold and copper providing two routes for CO elimination. Actually, the strong Au—Cu contact may result in charge transfers between both metals thus creating an electronic rich interface which is a suitable site for reactants adsorption and activation [39]. Indeed, the key point seems to be not only the gold assistance for the rapid formation of metallic copper but also the fact that gold supported on partially reduced copper (CuO$_x$) is an excellent catalysts for the water gas shift. Therefore, the advanced catalyst developed in this work is actually a thoughtful combination of two efficient catalysts for this reaction Au/CuO$_x$ and CuO-ZnO-Al$_2$O$_3$. The later prepared in a special manner using the double-layered oxides as precursor to guarantee an excellent metallic dispersion and to ensure a strong metal-oxide interaction.

In order to facilitate semi-quantitative comparison between our catalysts and some other standard systems for the WGS, the specific reaction rates in the model WGS mixture were calculated and presented in Table 3. All the rates were normalized by the active sites loading considering Au and Cu as the active components. The specific reaction rates values highlight the impact of gold as promoter of the low temperature WGS activity. Indeed, all the gold based catalysts presented a much higher reaction rate (around 40 times higher) than their homologues without gold. Furthermore, the developed catalysts are rather superior to highly active Au/Cu-CeO$_2$ systems recently reported in literature [42]. As shown in the table the studied catalysts present reaction rates which are more than 4 times higher than that exhibited for a Au/Cu-CeO$_2$ catalyst measured in the same reaction conditions.

For a practical application in the field of the fuel cell technology the catalysts must be tested in the presence of high concentrations of hydrogen and carbon dioxide. In this sense, Fig. 7 shows the catalytic activity of our gold based catalysts in the realistic post reforming mixture. Naturally, the conversion curves are shifted to
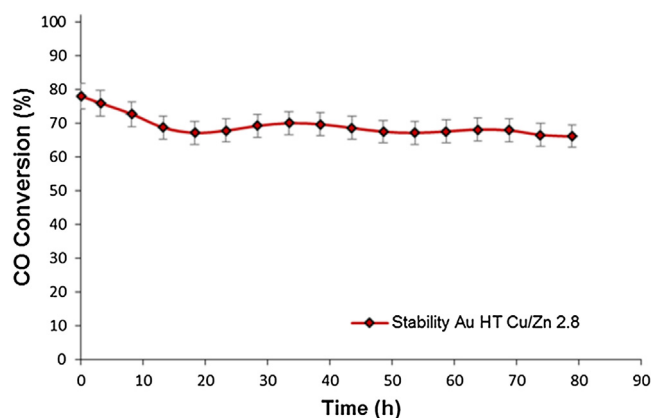
higher temperatures since the reactions products are now feed from the beginning of the process and the equilibrium is shifted in good agreement with the LeChetalier principle. Even so, the catalysts maintained elevated CO conversion reaching the thermodynamic limit around 250 °C in the best situation (sample HT 2.8). This fact represents also a valuable result from economical point of view.

3.7. Long thermal stability test

For a possible implementation of this type of catalysts in portable fuel processor they must be not only active but also sufficiently stable to long term operations. Therefore, the best catalyst (Au HT 2.8) was selected and submitted to a long stability test under "realistic" conditions (Fig. 8) at 230 °C. As show in the plot, the activity smoothly drops during the first 20 h of operation (the time required to achieve a steady state). Later on, the CO conversion becomes reasonably stable conserving high conversion (% CO) during 80 h of reaction. This is an encouraging result since apparently the Au/HT 2.8 catalysts does not get deactivated once reaching the steady state under a realistic post-reforming WGS mixture.

3.8. Start/stop cycles test

For portable applications, all the catalysts involved in the fuel processor (the reforming catalysts, and the WGS one) must tolerate the start-up/shut-down cycles of the engine. In fact, this type of start/stop stability proves are the most demanding test that can be imagined for a shift catalyst since during the stop stages the reactor is cooled down at room temperature with the reactive mixture flowing through the catalytic bed. The later involves that water may condensate on the catalystsí pores and deactivates the system. Despite this kind of tests seems essential for practical reasons they are not yet extended enough and only few reports can be found in literature considering these simulations [13,40–42]. Au/HT 2.8 was submitted to a 5 cycles of cooling down/heating up (Fig. 9). During the cooling down the reactor was kept at room temperature for 30 min to ensure the condensation of water on the catalytic bed. As presented in the plot the Au/HT 2.8 catalysts losses around 15% of CO conversion in the first 3 cycles. After 5 cycles the conversion remains stable at around 70% which is a high conversion level considering the hard conditions of the test. It can be then concluded that the Au/HT 2.8 is a rather robust catalysts that reasonably stands the start-up/shut-down operations. This result together with the elevated activity at low temperature and sufficient long term stability confirms the excellent features of these catalysts and their suitability for realistic applications.
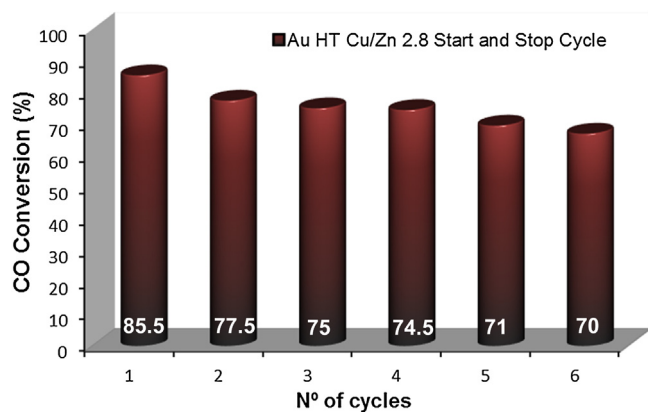
Fig. 9. Start/Stop cycles test of the Au/HT 2.8 catalyst.

4. Conclusions

A series of highly efficient catalysts for the WGS reaction has been prepared in this work. The materials consist on small gold nanoparticles supported on CuO-ZnO-Al$_2$O$_3$ mixed oxides obtained from hydrotalcite precursors. This type of precursor allows an ideal catalysts' microstructure and enhanced metal-oxide contact. The catalytic activity of these solids is guided by the Cu/Zn ratio being 2.8 an optimum balance. The samples display an advanced performance due to the Au—Cu synergy and its active participation in the reaction. The noble metal facilitates CuO reduction at early stages of the WGS ensuring the presence of two active phases Cu and Au almost from the begging of the process, without the need of previous pretreatment.

Under a "model" WGS mixture the catalysts achieve equilibrium conversion at very low temperature allowing high hydrogen production yield. The specific reaction rates underline the impact of gold in the catalytic activity remarking the outstanding performance of the developed catalysts. When a post-reforming mixture is considered the developed catalysts maintain elevated CO conversion, pointing their suitability for hydrogen clean up goals. Apart from the excellent conversions, the systems are stable for both long term and star-up/shut-down situations which is crucial prerequisite for a real application in fuel processor.

Overall, the combination of gold nanoparticles with the commercial-like Cu—Zn—Al formulation prepared from hydrotalcite precursor leads to a new generation of promising catalysts for the WGS reaction with potential impact in the development of hydrogen technology.

Acknowledgements

References

[1] R. Farrauto, S. Hwang, L. Shore, W. Ruettinger, J. Lampert, T. Giroux, Y. Liu, O. Ilinich, Annu. Rev. Mater. Res. 33 (2003) 1–27.
[2] G. Kolb, Fuel Processing for Fuel Cells, Wiley-VCH, Weinheim, 2008.
[3] V. Mehta, J.S. Copper, J. Powder Sources 114 (2003) 32–53.
[4] L. Wang, K. Murata, M. Inaba, J. Power Sources 145 (2005) 707–711.
[5] Dimitris K. Liguras, Dimitris I. Kondarides, Xenophon E. Verykios, Appl. Catal. B 43 (2003) 345–354.
[6] L.F. Bobadilla, V.C. Corberán, A.G. Avilés, S.M. González, S. Ivanova, M.I. Dominguez, F.R. Sarria, J.A. Odriozola, Appl. Catal. A 492 (2015) 38–47.
[7] G.W. Huber, J.W. Shabaker, J.A. Dumesic, Science 300 (2003) 2075–2077.
[8] L. Torrente-Murciano, F.R. Garcia-Garcia, Catal. Commun. 71 (2015) 1–6.
[9] C. Ratnasamy, J. Wagner, Catal. Rev. Sci. Eng. 51 (2009) 325–440.
[10] D.L. Trimm, Appl. Catal. A 296 (2005) 1–11.
[11] T.R. Reina, S. Ivanova, J.J. Delgado, I. Ivanov, V. Idakiev, T. Tabakova, M.A. Centeno, J.A. Odriozola, ChemCatChem 6 (2014) 1401–1409.
[12] M. Behrens, L. Kasatkin, S. Kuhl, G. Weinberg, Catal. Chem. Mater. 22 (2010) 386–397.
[13] T. Giroux, S. Hwang, Y. Liu, W. Ruettinger, L. Shore, Appl. Catal. B 55 (2005) 185–200.
[14] R.J. Farrauto, Y. Liu, W. Ruettinger, Catal. Rev. Sci. Eng. 49 (2007) 141–196.
[15] M.G. Castaño, T.R. Reina, S. Ivanova, M.A. Centeno, J.A. Odriozola, J. Catal. 314 (2014) 1–9.
[16] Q. Fu, H. Saltsburg, M. Flytzani-Stephanopoulos, Science 310 (2003) 935–938.
[17] D. Andreeva, V. Idakiev, T. Tabakova, L. Ilieva, P. Falaras, A. Bourlinos, A. Travlos, Catal. Today 72 (2002) 51–57.
[18] B. Bhaduri, N. Verma, Catal. Lett. 145 (2015) 1262–1271.
[19] J.A. Rodriguez, Catal. Today 160 (2011) 3–10.
[20] J. He, M. Wei, B. Li, Y. Khang, D.G. Evans, X. Duan, Struct. Bond. 119 (2006) 89–119.
[21] A. Tsyganok, A. Sayari, J. Solid State Chem. 179 (2006) 1830–1841.
[22] S. Ivanova, C. Petit, V. Pitchon, Appl. Catal. A 267 (2004) 191–201.
[23] T.R. Reina, A. Alvarez, S. Ivanova, J.A. Odriozola, M.A. Centeno, ChemCatChem 4 (2012) 512–520.
[24] M. Jitianu, M. Balasoiu, M. Zaharescu, A. Jitianu, A. Ivanov, J. Sol–Gel Sci. Technol. 19 (2000) 453–457.
[25] F. Cavani, F. Trifirò, A. Vaccari, Catal. Today 11 (1991) 173–301.
[26] J.T. Kloprogge, L. Hickey, R.L. Frost, J. Solid State Chem. 177 (2004) 4047–4057.
[27] S.J. Palmer, R.L. Frost, L.M. Grand, J. Raman Spectrosc. 42 (2011) 1168–1173.
[28] R.L. Frost, A. Soisnard, N. Voyer, S.J. Palmer, W.N. Martens, J. Raman Spectrosc. 40 (2009) 645–649.
[29] G.J. Millar, I.H. Holm, P.J.R. Uwins, J. Drennan, J. Chem. Soc. Faraday Trans. 94 (1988) 593–600.
[30] J.F. Xu, W. Ji, Z.X. Shen, S.H. Tang, X.R. Ye, D.Z. Jia, X.Q. Xin, J. Solid State Chem. 147 (1999) 516–519.
[31] W. Wang, Q. Zhou, X. Fei, Y. He, P. Zhang, G. Zhang, L. Peng, W. Xie, Cryst. Eng. Commun. 12 (2010) 2232–2237.
[32] D. Simeone, C. Dodane-Thiriet, D. Gosset, P. Daniel, M.J. Beauvy, Nucl. Mater. 300 (2002) 151–160.
[33] H. Cynn, S.K. Sharma, T.F. Cooney, M. Nicol, Phys. Rev. B 45 (1992) 500.
[34] L. Hea, L. Chenga, G. Lianga, Y. Yu, F. Zhao, Appl. Catal. A 452 (2013) 88–93.
[35] I. Melian-Cabrera, M. López Granados, J.L.G. Fierro, J. Catal. 210 (2002) 273–284.
[36] R. Burch, Phys. Chem. Chem. Phys. 8 (2006) 5483–5500.
[37] H. Sakurai, T. Akita, S. Tsubota, M. Kiuchi, M. Haruta, Appl. Catal. A 291 (2005) 179–187.
[38] M.M. Schubert, S. Hackenberg, A.C. Van Veen, M. Muhler, V. Plzak, R.J. Behm, J. Catal. 197 (2001) 113–122.
[39] Y. Li, Q. Fu, M. Flytzani-Stephanopoulos, Appl. Catal. B 27 (2000) 179–191.
[40] O.F. Arbelaez, T.R. Reina, S. Ivanova, F. Bustamante, A.L. Villa, M.A. Centeno, J.A. Odriozola, Appl. Catal. A: Gen. 497 (2015) 1–9.
[41] S. Collussi, L. Katta, F. Amoroso, R.J. Farrauto, A. Trovarelli, Catal. Commun. 47 (2014) 63–66.
[42] T. Reina, S. Ivanova, M.A. Centeno, J.A. Odriozola, Appl. Catal. B: Environ. 187 (2016) 98–107.